RESEARCH ARTICLE

The Relaxed Eddy Accumulation Method Over the Amazon Forest: The Importance of Flux Strength on Individual and Aggregated Flux Estimates

Nelson Luís Dias[1] [ORCID] · **Ivan Mauricio Cely Toro[2]** · **Cléo Quaresma Dias-Júnior[2]** · **Luca Mortarini[3,4]** · **Daiane Brondani[5]**

Abstract

The ability of the relaxed eddy accumulation (REA) method to estimate the kinematic fluxes of temperature, water vapor and carbon dioxide was assessed for the dry season (3 months) at the ATTO (Amazon Tall Tower Observatory) site from turbulence measurements. The measurements were performed at 50 m above ground within the roughness sublayer. Non-conformity with inertial sublayer conditions was confirmed one more time by analyzing dimensionless scalar standard deviations. Over the scale of the whole dry season, REA and EC (eddy covariance) estimates are essentially equal. Recently found results that the REA method outperforms Monin–Obukhov-based approaches are confirmed. However, we also verify that such results fail to reveal significant variability and scatter of the REA estimates when the fluxes are of small magnitude. On the basis of previous studies, we conjecture that this is caused by a likely imbalance between scalar gradient production and molecular dissipation. Confirmation of our results to trace gases, therefore, requires further study.

✉ Nelson Luís Dias
  nldias@ufpr.br

  Ivan Mauricio Cely Toro
  mauriciocelytoro@gmail.com

  Cléo Quaresma Dias-Júnior
  cleo.quaresma@ifpa.edu.br

  Luca Mortarini
  l.mortarini@isac.cnr.it

  Daiane Brondani
  meteorologia.daia@gmail.com

[1] Department of Environmental Engineering, Federal University of Paraná, Curitiba, Brazil

[2] Department of Physics, Federal Institute of Pará, Belém, Brazil

[3] Universidade Federal de Santa Maria, Santa Maria, RS, Brazil

[4] Institute of Atmospheric Sciences and Climate, National Research Council (ISAC-CNR), Torino, Italy

[5] Department of Pure and Applied Sciences (DiSPeA), University of Urbino "Carlo Bo", Urbino, Italy

1 Introduction

The relaxed eddy accumulation (REA) method, proposed by Businger and Oncley (1990), is a simplification of the Eddy Accumulation Method conceived by Desjardins (1972, 1977). The most important feature of the REA method from the experimental point of view is that it does not require a fast-response instrument to measure the scalar concentration s whose turbulent flux is wanted. Instead, the sign of the vertical velocity w is used in real time to switch a valve drawing air at a constant flow rate into two different reservoirs. At the end of a block of measurement, the mean concentration of the scalar can be measured by a slow-response sensor in each of the reservoirs. In this work, note that the REA method is actually simulated using fast-response sensors.

The REA method has gained wide use to measure surface fluxes of substances for which fast-response gas analyzers are either non-existent or impractical. In that capacity, it has been reported to measure isoprene (Bowling et al. 1998), ammonia (Zhu et al. 2000), terpenoid (Mochizuki et al. 2014) and ethene, propene, buthene and isoprene (Rhew et al. 2017) fluxes, to cite but a few.

The REA predicts the scalar turbulent flux from:

$$\overline{w's'} = \beta_s \sigma_w (\overline{s^+} - \overline{s^-}), \tag{1}$$

where $\overline{s^+} = \overline{[s|w > 0]}$ and $\overline{s^-} = \overline{[s|w < 0]}$ are the conditional means of s on the sign of the vertical velocity w (under the assumption that $\overline{w} = 0$, so that $w = w'$), and the overbars and primes are standard notation for Reynolds' decomposition into a mean and the fluctuation around it. In the present work all means are taken over 30-min blocks. For conciseness, we denote $\overline{s^+} - \overline{s^-}$ by $\Delta \overline{s}$.

From its inception, it has been recognized that under validity of Monin–Obukhov similarity theory (MOST), β_s should be a function of Obukhov's stability variable ζ (Businger and Oncley 1990); several studies have found $\beta_s \approx 0.6$ with a modest variation of $\approx 10\%$ over a wide range of stabilities when the measurements are made in the inertial sublayer of the atmospheric surface layer (see, for example, Businger and Oncley 1990; Baker et al. 1992; Katul et al. 2018).

Over forests, an important issue is to estimate the fluxes from the canopy to the atmosphere of volatile organic compounds (VOCs) such as isoprene; this is particularly critical in the Amazon, where secondary organic aerosols have a significant role in the formation of cloud condensation nuclei (CCNs) (Fuentes et al. 2016). Here, due to the aforementioned difficulty of measuring VOC concentrations with fast-response instruments, the REA method can have a significant impact on closing the knowledge gap on VOC emission rates from the forest. It is also noteworthy that new, better and cheaper technologies for *in-situ* analysis of $\Delta \overline{s}$ are emerging that leverage the applicability of the REA method (Sarkar et al. 2020).

Invariably, REA measurements require a sonic anemometer measuring w at high frequency to control in real time the valve switching the flow of air into two reservoirs for the measurement of $\overline{s^+}$ and $\overline{s^-}$ at the end of an averaging period. This means that simultaneous measurements of sonic temperature θ are available, allowing standard eddy covariance (EC) measurements of $\overline{w'\theta'}$. This in turn means that, for each block, β_θ can be calculated from (1) with $s = \theta$. Therefore, if the scalar s of interest is perfectly correlated to temperature, β_s may be allowed to vary from block to block by setting $\beta_s = \beta_\theta$ for each block. This strategy,

which we call "REA-T " (where "T " stands for auxiliary sonic temperature measurements) appears to have originated with Bowling et al. (1998), and is in wide use (Ren et al. 2011; Mochizuki et al. 2014; Rhew et al. 2017; Sarkar et al. 2020, etc.). Alternatively, of course, one can still adopt a single value of β_s (which we call "REA-S", where "S" stands for "single value") based on measurements of s with eddy covariance (using instrumentation with adequate response time) or again an assumption of similar behavior with more easily measured quantities.

Either way, the REA invokes (i) an assumption of similarity between scalars, or (ii) the validity of MOST for the scalar of interest or (iii) at least the constancy of β_s even if MOST does not apply. Strictly speaking, it is known that if MOST is valid for any pair of scalars, their similarity functions must be the same, and their correlation must be perfect (Hill 1989; Dias and Brutsaert 1996; Dias 2013). Most of the time, therefore, either (i) or (ii) seems to be warranted for measurements made in the inertial sublayer of the atmospheric boundary layer, where MOST is assumed to hold over homogeneous surfaces with sufficient fetch.

However, even under these conditions, recently evidence has emerged that MOST may not be universally valid for *all* scalars, but rather that it appears to depend on the equilibrium between gradient production and dissipation of scalar semivariance: the presence of relatively large values of other terms in the scalar semivariance budget, such as the storage or the transport terms, can seriously disrupt MOST conformity for the scalar in question (Zahn et al. 2023). Interestingly, in the same study Zahn et al. (2023) have found that the REA method is much superior to the variance method (a classical MOST indirect method to estimate scalar fluxes) even when equilibrium between gradient production and molecular dissipation does not hold for the scalar, which suggests that in this case (iii) may be valid at least on average.

In the roughness sublayer (RSL) over a forest there is strong evidence of large departures of scalar behavior from MOST (Dias et al. 2009; Zahn et al. 2016b; Chor et al. 2017). Zahn et al. (2016b) found large departures for all 3 scalars (temperature, H_2O and CO_2) measured at the ATTO (Amazon Tall Tower Observatory) site in Central Amazonia (see description below), but noted that scalar similarity improved significantly for small zenith angles. They also found considerable scatter in the β_s values, which again was reduced for small zenith angles, which happen in the middle of the day, when the scalar fluxes tend to be largest in absolute value. In order to be concise, in this work we call fluxes which are large in absolute value "large-magnitude" fluxes.

Chor et al. (2017) equally found strong dissimilar behavior for the same scalars, as well as wide scatter in their Monin–Obukhov integral similarity functions. This casts doubt on the applicability of the REA method in any of the two forms (β_s constant or $\beta_s = \beta_\theta$ for each block) mentioned above, while at the same time is at odds with the recent findings of Zahn et al. (2023) of good REA performance, although the latter were obtained for a lake, not a forest.

Using a large dataset recently measured at the ATTO site, this work therefore has the objective to clarify some of the issues mentioned above: the main point of investigation is to try to elucidate how β_s can have significant variability as disclosed by Zahn et al. (2016b) while at the same time the REA method can have a very good performance as found by Zahn et al. (2023). In particular, we seek to answer the following questions:

1. How close to constant is β_s (i.e. what its typical scatter is) in comparison with the results by Zahn et al. (2016b)?
2. To what extent do the dimensionless vertical velocity and scalar standard deviations follow MOST in the roughness sublayer? These functions have been shown by Zahn et al. (2023) to jointly explain the near-constancy of β_s under MOST.

3. How good are block-by-block REA flux estimates in the Amazonian roughness sublayer in comparison to eddy-covariance measurements?
4. Since block-by-block errors may be reduced by averaging if they are not strongly biased, how good is the REA method (in comparison with eddy-covariance) for "long-term" (of the order of many days to a whole season), "mean" flux estimates?

The relevant relationships among the quantities of interest in this work are reviewed in Sect. 2; the ATTO site and details of data processing are given in Sect. 3; results for similarity functions are analyzed in Sect. 4, and for the actual prediction of fluxes in Sect. 5. Discussion and conclusions are given in Sect. 6.

2 Methods

Since the "variance method" has shown to be a good indicator of the breakdown of MOST in the RSL (Dias et al. 2009; Zahn et al. 2016b; Chor et al. 2017; Dias-Júnior et al. 2019), and even in a classical inertial sublayer (Zahn et al. 2023), we test its standard form:

$$\frac{\sigma_s}{s_*} = \phi_{\sigma_s}(\zeta),\tag{2}$$

with:

$$u_*^2 = -\overline{u'w'},\tag{3}$$

$$\zeta = -\frac{\kappa g(z - d_0)\theta_*}{\overline{\theta}u_*^2},\tag{4}$$

$$u_* s_* = \overline{w's'},\tag{5}$$

$$\sigma_s = \sqrt{\overline{s's'}},\tag{6}$$

where u is the longitudinal velocity, z is the measurement height, and d_0 is the zero-plane displacement height.

In the case of the REA method, it can be readily seen by rearranging (1) that (see Zahn et al. 2023, Eq. (17)):

$$\frac{1}{\beta_s} = \frac{\sigma_w \Delta \overline{s}}{\overline{w's'}} = \frac{\sigma_w}{u_*}\frac{\Delta \overline{s}}{s_*} = \phi_{\sigma_w}(\zeta)\phi_{\Delta \overline{s}}(\zeta),\tag{7}$$

where $\sigma_w/u_* = \phi_{\sigma_w}(\zeta)$ and $\Delta \overline{s}/s_* = \phi_{\Delta \overline{s}}(\zeta)$, and that β_s is a MOST function under ideal conditions.

Regarding (1), (2) and (7), two points are concerned:

1. Experimentally, "to be or not to be" a funcion of ζ is largely a matter of assessing the goodness-of-fit of data to a proposed model. Although this is seldom—if at all—done in practice for MOST functions (to the best of our knowledge), it is possible to quantify such goodness-of-fit by standard statistical indices. Therefore, in this study we compare quantitatively ϕ_{σ_w}, ϕ_{σ_s} and $\phi_{\Delta \overline{s}}$ as described in the sequence.
2. As we will see in Sect. 4, the quality of the $\phi(\zeta)$s or even the variability of β_s do not translate directly to the quality of the estimated fluxes $\overline{w's'}$ over different time scales (block-by-block or longer term). Therefore, a second quantitative assessment must be made of the quality of the estimated fluxes themselves.

Besides graphical comparisons, we compare predicted (y) to observed (x) values using standard statistics: coefficient of correlation r, coefficient of determination C_d, BIAS, mean

absolute error MAE, root mean square error RMSE, their normalized versions NBIAS, NMAE, NRMSE, and Willmott's refined index of model performance d_r (Willmott et al. 2012). An important issue here is that small magnitudes of predicted and observed fluxes tend to be masked both graphically in traditional "$x \times y$" plots and statistically when directly quantified, say, by RMSE or MAE. For this reason, the normalized versions are better to discern "relative" errors. For the sake of completeness, these quantities are:

$$r = \frac{\text{Cov}(x, y)}{\sigma_x \sigma_y}, \qquad\qquad C_d = 1 - \frac{\text{MSE}}{\sigma_x^2}, \qquad (8)$$

$$\text{BIAS} = \frac{1}{n} \sum_{i=1}^{n} (y_i - x_i), \qquad\qquad \text{NBIAS} = \frac{\text{BIAS}}{|\overline{x}|}, \qquad (9)$$

$$\text{MAE} = \frac{1}{n} \sum_{i=1}^{n} |y_i - x_i|, \qquad\qquad \text{NMAE} = \frac{\text{MAE}}{|\overline{x}|}, \qquad (10)$$

$$\text{RMSE} = \left[\frac{1}{n} \sum_{i=1}^{n} (y_i - x_i)^2 \right]^{1/2}, \qquad\qquad \text{NRMSE} = \frac{\text{RMSE}}{|\overline{x}|}, \qquad (11)$$

where $\text{Cov}(x, y)$ is the covariance between predicted and observed values, σ_x and σ_y are their standard deviations, $\overline{x}$ is the mean of the observed values, and $\text{MSE} = \text{RMSE}^2$ is the mean square error. Note that if all predicted values are equal, r makes no sense because $\sigma_y = 0$. Willmott's refined index of performance is:

$$d_r = \begin{cases} 1 - \frac{\sum_{i=1}^{n} |y_i - x_i|}{2 \sum_{i=1}^{n} |x_i - \overline{x}|}, & \sum_{i=1}^{n} |y_i - x_i| \leq 2 \sum_{i=1}^{n} |x_i - \overline{x}|, \\ \frac{2 \sum_{i=1}^{n} |x_i - \overline{x}|}{\sum_{i=1}^{n} |y_i - x_i|} - 1, & \sum_{i=1}^{n} |y_i - x_i| > 2 \sum_{i=1}^{n} |x_i - \overline{x}|. \end{cases} \qquad (12)$$

3 Experimental Site and Data

In this work we used data collected at a micrometeorological tower built up at the experimental ATTO (Amazon Tall Tower Observatory) site, in Central Amazon, in a *terra firme* forest, approximately 150 km northeast from the city of Manaus—AM, Brazil. At the site, there are two towers that are situated on an extensive plateau area (130 m above sea level) immersed in a large primary forest (see Fig. 1). The vegetation is typical of undisturbed *terra firme* forest. The average height of the vegetation is approximately 30–40 m and the leaf area index is around 5–6 $m^2 \, m^{-2}$. The predominant wind is from the northeast (Andreae et al. 2015; Santana et al. 2018).

There are two towers at the ATTO site, known as the (main) ATTO tower (02° 08′ 45″ S, 59° 00′ 20″ W) with a height of 325 m and the "Instant" tower (02° 08′ 39″ S, 59° 00′ 00″ W) with a height of 81 m (Dias-Júnior et al. 2019). The experimental setup is shown in Fig. 2. The redundant data used in this work were collected during the months of August, September, and October 2021. These months correspond to the dry season in the Amazon region. The data were measured at 10 Hz by a sonic anemometer (model CSAT3B, Campbell Scientific, Inc) and an open-path gas analyzer (model LICOR 7500A LI-COR Inc), both installed 50 m above the ground at the Instant tower.

The dataset was divided in 3959 30-min data blocks. A quality control analysis similar to the one described in Zahn et al. (2016a) was applied to u, v, w (velocity components of the sonic anemometer), θ (sonic temperature), ω_q (H_2O molar density) and ω_c (CO_2 molar
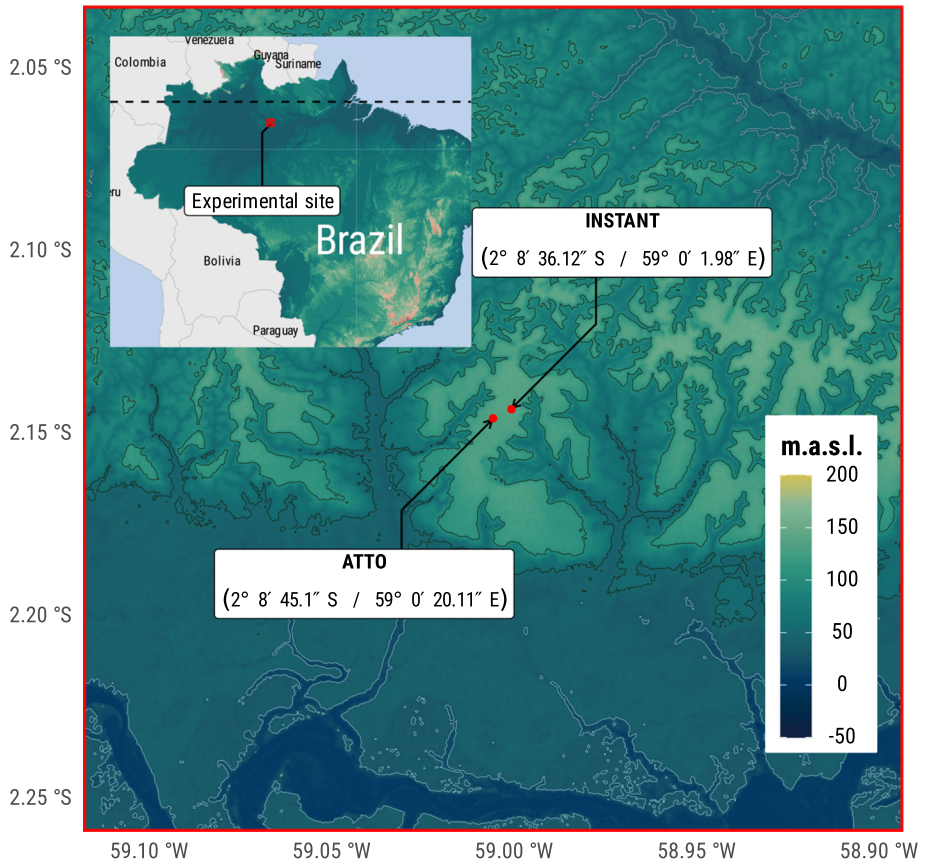
Fig. 1 Overall location of the ATTO site

density) for each block. The procedure divides a block with n data points ($n = 18{,}000$ in our case) into $n_s = n/m$ sub-blocks with m points each. One-minute sub-blocks, $m = 600$, were used. Before quality control, missing or erroneous data were flagged as NANs; then, for each sub-block, the median $\widetilde{x}_k$ and the mean absolute deviation (MAD_k) around it,

$$\mathrm{MAD}_k = \frac{1}{m} \sum_{i=0}^{m-1} |x_{km+i} - \widetilde{x}_k| \tag{13}$$

were evaluated. The sub-block index, k, runs from 0 to $n_s - 1$. For each sub-block:

- A spike is identified each time $|x_{km+i} - \widetilde{x}_k| > 5\,\mathrm{MAD}_k$;
- a locking condition (i.e. x_i varies too little over a sub-block) is identified if $\max_k(\mathrm{MAD}_k) < 0.01$ (K for θ, m s^{-1} for u, v and w and mmol m^{-3} for ω_q and ω_c);
- a non-stationary condition is identified if the difference between the maximum and minimum sub-block medians is larger than Q_x, where $Q_{u,v} = 5\,\mathrm{m\,s^{-1}}$, $Q_w = 3\,\mathrm{m\,s^{-1}}$, $Q_\theta = 5$ K, $Q_{\omega_q} = 300\,\mathrm{mmol\,m^{-3}}$ and $Q_{\omega_c} = 10\,\mathrm{mmol\,m^{-3}}$.

When all the above conditions were met, the following criteria were applied sequentially:
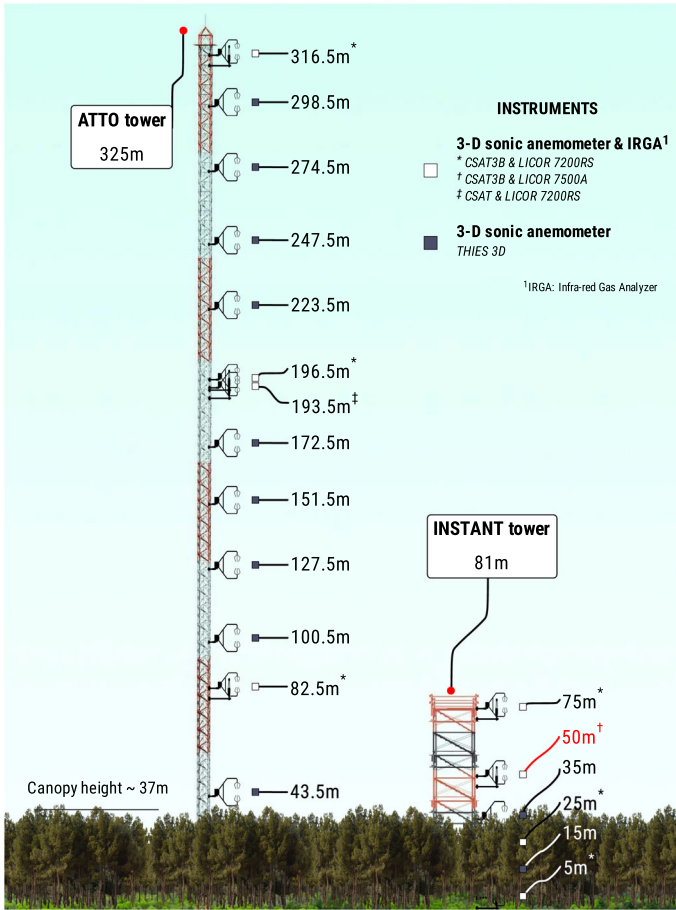
Fig. 2 Instrument setup of the ATTO site. In this work, only the 50-m data from the Instant Tower were used

1. If the number of values equal to NAN in the block was more than 1% of the block size, all x_i were set to NAN and the block was effectively discarded;
2. All spikes were flagged as NAN. After that, if the number of values equal to NAN in the block was more than 1% of the block size, all x_i were set to NAN and the block was effectively discarded;
3. If a locking condition and/or a non-stationary condition were identified, all the half-hour block was set to NAN and again discarded from the analysis;
4. If the block was not discarded, all runs of NANs in x were linearly interpolated from the valid extremities.

After conducting the quality control analysis, we obtained 1146 blocks of 30 min each for ω_c, 1163 blocks for ω_q, 1307 blocks for θ, u, v, and w. In addition, we computed the half-hourly mean values of turbulence statistics by applying two coordinate rotations (McMillen 1988) to ensure that the average lateral and vertical velocities were zero. For all subsequent analyses the H_2O and CO_2 molar densities ω_q and ω_c were converted to instantaneous mass concentrations using the pressure sensor from the LI7500 (see for instance Edson et al.

[2011](#)). In this work they are reported as q in $\mathrm{g\,kg^{-1}}$ and c in $\mathrm{mg\,kg^{-1}}$ respectively. Note that covariances calculated with mass concentrations dispense with the WPL density corrections (Webb et al. [1980](#)).

4 Results for Similarity Functions

4.1 Similarity Functions for the Classical Standard Deviation Statistics

Standard inertial sublayer (ISL) predictions for ϕ_{σ_w} and ϕ_{σ_s} are (Chor et al. [2017](#)):

$$\phi_{\sigma_w}(\zeta) = \begin{cases} 1.25(1 - 3\zeta)^{1/3}, & \zeta < 0, \\ 1.25, & \zeta \geq 0, \end{cases} \tag{14}$$

$$\phi_{\sigma_s}(\zeta) = \begin{cases} 2(1 - 9.5\zeta)^{-1/3}, & \zeta < 0, \\ 2, & \zeta \geq 0. \end{cases} \tag{15}$$

When calculating the statistics σ_s/s_*, we further filtered the data with sign restrictions for each scalar and stability condition. Thus, in the case of θ, we only use $\Delta\overline{\theta} < 0$ for stable conditions ($\theta_* < 0$) and $\Delta\overline{\theta} > 0$ for unstable conditions ($\theta_* > 0$); for q, we only use positive values of $\overline{w'q'}$ and only positive values of both $\Delta\overline{q}$ and q_* for both stable and unstable conditions; and in the case of c we only use $\Delta\overline{c} > 0$ for stable conditions, with $c_* > 0$, and $\Delta\overline{c} < 0$ for unstable conditions, with $c_* < 0$. The further restrictions on the signs of $\Delta\overline{s}$ were imposed so that exactly the same data sets were used for both similarity functions ϕ_{σ_s} and $\phi_{\Delta\overline{s}}$, and therefore corresponding statistics and figures can be compared.

Figure [3](#) shows the statistics σ_w/u_*, and σ_s/s_* for $s = \theta$, $s = q$ and $s = c$ for stable and unstable conditions, respectively. The findings of Zahn et al. ([2016b](#)) and Chor et al. ([2017](#)) for the ATTO site (but generally valid for the roughness sublayer over forests) are confirmed: overall, there is an excess of scalar variance in comparison to flux (actually s_*), giving strong indication that gradient production of $\overline{s's'}/2$ often is far less than scalar molecular dissipation (see Zahn et al. [2023](#)); however, a detailed analysis of the semivariance scalar budgets falls outside of our scope. The σ_w/u_* statistics are somewhat less "well-behaved" than those obtained by Zahn et al. ([2016b](#)) and Chor et al. ([2017](#)) for the same site: under unstable conditions, there is a clear tendency for many blocks to display *less* variance in comparison to flux (actually u_*), suggesting that now a part of the gradient and buoyant production of TKE (turbulence kinetic energy) is being "exported" rather than dissipated locally. This is indicative of a negative transport of TKE in the RSL above the canopy (see Fig. 1b of Chamecki et al. [2020](#), and Mortarini et al. [2023](#)).

Besides the standard ISL versions of $\phi_\sigma(\zeta)$ shown in blue, we also obtained least-squares (using the Levenberg–Marquardt algorithm) estimates depicted in vermillion in Fig. [3](#) with the general forms:

$$\phi_{\sigma_w}(\zeta) = a_w(1 - b_w\zeta)^{1/3}, \qquad \zeta < 0, \tag{16}$$

$$\phi_{\sigma_w}(\zeta) = c_w, \qquad \zeta \geq 0, \tag{17}$$

$$\phi_{\sigma_s}(\zeta) = a_s(1 - b_s\zeta)^{-1/3}, \qquad \zeta < 0, \tag{18}$$

$$\phi_{\sigma_s}(\zeta) = c_s, \qquad \zeta \geq 0. \tag{19}$$

The Levenberg–Marquard estimates were obtained with the built-in functionality available in the Gnuplot plotting program (www.gnuplot.info). The values of the fitted coefficients are
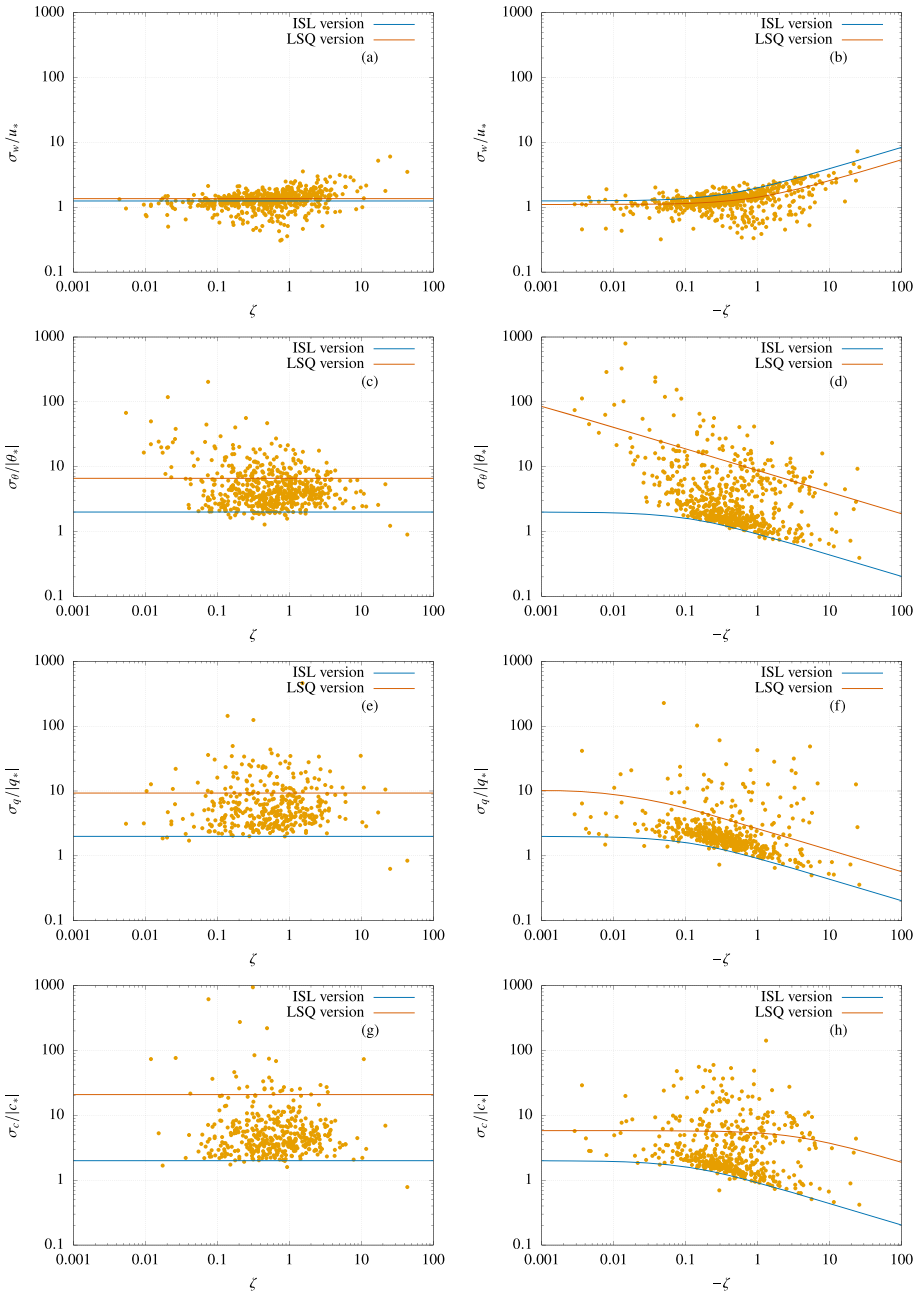
Fig. 3 Dimensionless values of σ_w/u_* (**a, b**) and σ_s/s_* for $s = \theta$ (**c, d**), $s = q$ (**e, f**) and $s = c$ (**g, h**), for stable (**a, c, e, g**) and unstable (**b, d, f, h**) conditions. The blue line is the standard inertial sublayer (ISL) prediction and the vermillion line is a least-squares (LSQ) fit

Table 1 Least-squares estimates of coefficients for $\phi_{\sigma_w}(\zeta)$ and $\phi_{\sigma_s}(\zeta)$ for $s = \theta, q, c$

Variable	a	b	c
w	1.10165	1.16823	1.35626
θ	198.159	11,677.3	6.62063
q	10.3842	60.4992	9.2982
c	5.81503	0.282431	20.8740

Table 2 Performance statistics for the LSQ functions $\phi_{\sigma_w}(\zeta)$ and $\phi_{\sigma_s}(\zeta)$ for $s = \theta, q, c$

Variable	r	C_d	BIAS	MAE	RMSE	d_r
Stable conditions						
w	–	− 0.0005	− 0.0136	0.3252	0.5960	0.5025
θ	–	− 0.0017	− 4.7657	9.1976	116.0751	0.6305
q	–	0.0000	0.0328	7.4703	25.5382	0.4988
c	–	0.0000	0.0896	28.7691	184.8037	0.4987
Unstable conditions						
w	0.6266	0.3918	0.0035	0.2721	0.4146	0.5922
θ	0.3802	0.0905	4.1461	12.7000	37.3868	0.4089
q	0.1046	0.0099	− 0.1111	3.6544	12.2497	0.5046
c	0.0481	0.0023	0.0028	4.9854	10.0601	0.4983

For stable conditions, the ϕ_σs are constant and r cannot be calculated

given in Table 1. As it can be seen both visually and from the coefficients in the table, the fitted (LSQ) versions differ significantly from their ISL counterparts, but by definition they still provide the "best fits". Note that the large excursions of a relatively small percentage of points can have a significant impact on the estimates of a, b and c; however, there is no clear cutoff point nor are there visible outliers: for this reason, they are all retained. These coefficients should be considered specific for this dataset. They are used here only because they provide the best statistics for the dimensionless standard deviations, and should not be considered in any way representative of RSL statistics.

Table 2 shows the performance statistics obtained for the LSQ versions (not the ILS versions) of the similarity functions ϕ_{σ_w} and ϕ_{σ_s}. Note that these funcions are all dimensionless, so there is no need to calculate normalized performance statistics. The statistics confirm the visual impression that, particularly for the scalars, the dimensionless standard deviations perform rather poorly, with generally small correlations between data points and predicted ϕ_{σ_s}s, and large values of MAE and RSME (for dimensionless functions, a good outcome would be MAE, RMSE ~ 0.1).

4.2 Similarity Functions for the REA Statistics

Figure 4 shows the statistics of $\Delta\bar{s}/s_*$ and the similarity functions $\phi_{\Delta\bar{s}}(\zeta)$ fitted by least squares. The same general form of (18)–(19) was used:

$$\phi_{\Delta\bar{s}}(\zeta) = a_{\Delta\bar{s}}(1 - b_{\Delta\bar{s}}\zeta)^{-1/3}, \quad \zeta < 0, \tag{20}$$

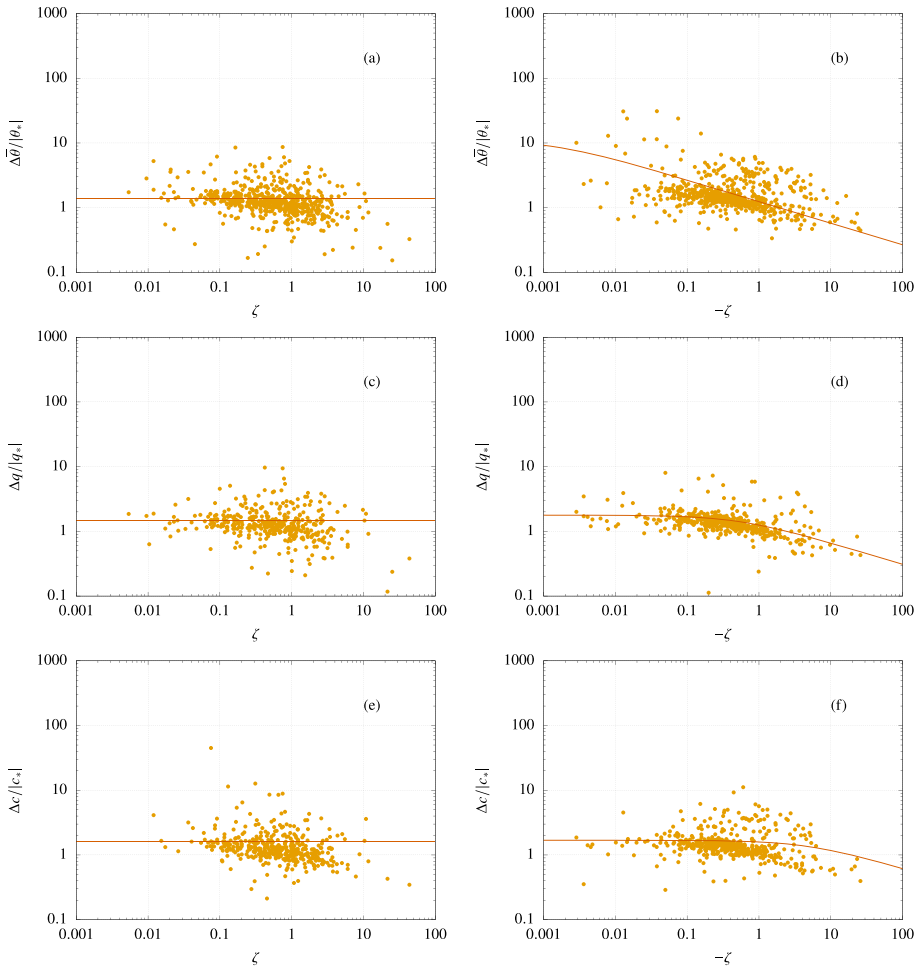$$\phi_{\Delta\bar{s}}(\zeta) = c_{\Delta\bar{s}}, \quad \zeta \geq 0. \tag{21}$$

Fig. 4 Dimensionless values of $\Delta\bar{s}/s_*$ for $s = \theta$ (**a, b**), $s = q$ (**c, d**) and $s = c$ (**e, f**) for stable (**a, c, e**) and unstable (**b, d, f**) conditions. The vermillion line is a least-squares (LSQ) fit

Variable	a	b	c
θ	11.0134	696.671	1.41422
q	1.77867	1.87614	1.45977
c	1.68775	0.197135	1.59717

Table 3 Least-squares estimates of coefficients for $\phi_{\Delta\bar{s}}(\zeta)$ for $s = \theta, q, c$

The corresponding values are shown in Table 3.

Because these functions have only been explicitly proposed very recently by Zahn et al. (2023), these may be the first results obtained in a roughness sublayer over a forest. Visually, the $\phi_{\Delta\bar{s}}$ values are signficantly less scattered than their ϕ_{σ_s} counterparts, indicating that REA dimensionless statistics may be potentially more useful than standard deviation ones. This is confirmed quantitatively in Table 4, where MAE and RMSE for the $\phi_{\Delta\bar{s}}$s are at

Table 4 Performance statistics for the LSQ functions $\phi_{\Delta \overline{s}}(\zeta)$ for $s = \theta, q, c$

Variable	r	C_d	BIAS	MAE	RMSE	d_r
Stable conditions						
θ	–	-0.0016	-0.2583	0.8142	6.3857	0.5670
q	–	0.0000	0.0033	0.5875	0.9930	0.4991
c	–	0.0000	0.0034	0.7760	2.4356	0.4989
Unstable conditions						
θ	0.3237	0.1011	-0.0653	1.0226	2.3101	0.4938
q	0.3020	0.0902	-0.0041	0.3511	0.7237	0.5651
c	0.1240	0.0149	0.0014	0.5984	1.0185	0.4998

For stable conditions, the ϕ_{σ_s}s are constant and r cannot be calculated

least an order of magnitude less than the corresponding values in Table 2. Clearly, the REA dimensionless statistics behave better (as a "function" of ζ) in the roughness sublayer than their dimensionless standard deviation counterparts: a physical explanation for this is not at hand and will require further research. However, the scatter is still relatively large and this is probably a consequence of measurements made within the RSL.

5 Results for Predicted Fluxes

5.1 Flux Estimates from Dimensionless Standard Deviations (Variance Method)

When MOST does not apply for a particular scalar s, it makes little sense to estimate its turbulent fluxes from the standard deviation similarity function $\phi_{\sigma_s}(\zeta)$, given the unacceptable scatter seen in Fig. 3 and the corresponding performance statistics in Table 2. Here, we re-do this exercise not because it is applicable in practice for our site, but because (a) it highlights the role of large magnitude fluxes on visual and numerical evaluation of the results; and (b) it provides a baseline to assess the gains in applying the REA method, as done by Zahn et al. (2023). We estimate the fluxes $\overline{w's'}$ using the observed values of u_*; an iterative procedure is performed for $s = \theta$ by starting at $\zeta = 0$ and calculating θ_* (from Eq. (2)) and ζ (from Eq. (4)) until convergence in θ_*; and then q_* and c_* are obtained again from Eqs. (2) and (4). All kinematic fluxes are then obtained from Eq. (5). Note that we are using the whole dataset both for estimating the coefficients a, b and c in (18)–(19) and for evaluating the performance of the estimated fluxes, since our intention here is only to assess the *relative* merits of the variance and REA methods.

Figure 5 shows the kinematic fluxes predicted by the variance method. For θ under unstable conditions, the predicted fluxes are much smaller in magnitude than the observed ones. This means that $\zeta \approx 0$ always for the prediction of the other two fluxes. In spite of that, we see that there is always a linear trend (and often a large linear correlation) between observed and predicted values. The corresponding performance statistics are given in Table 5. The very large magnitude of the errors is clearly discernible by the (large) values of NBIAS, NMAE and NRMSE.

The spread of the small fluxes is difficult to discern in Fig. 5. To emphasize the *relative* error made in flux estimation, we re-plot the same results in Fig. 6. Now we plot the ratios of predicted to observed fluxes in the vertical axes, against the observed fluxes in the horizontal axes. The blue lines are the medians of the ratios. The figure shows how the large magnitude
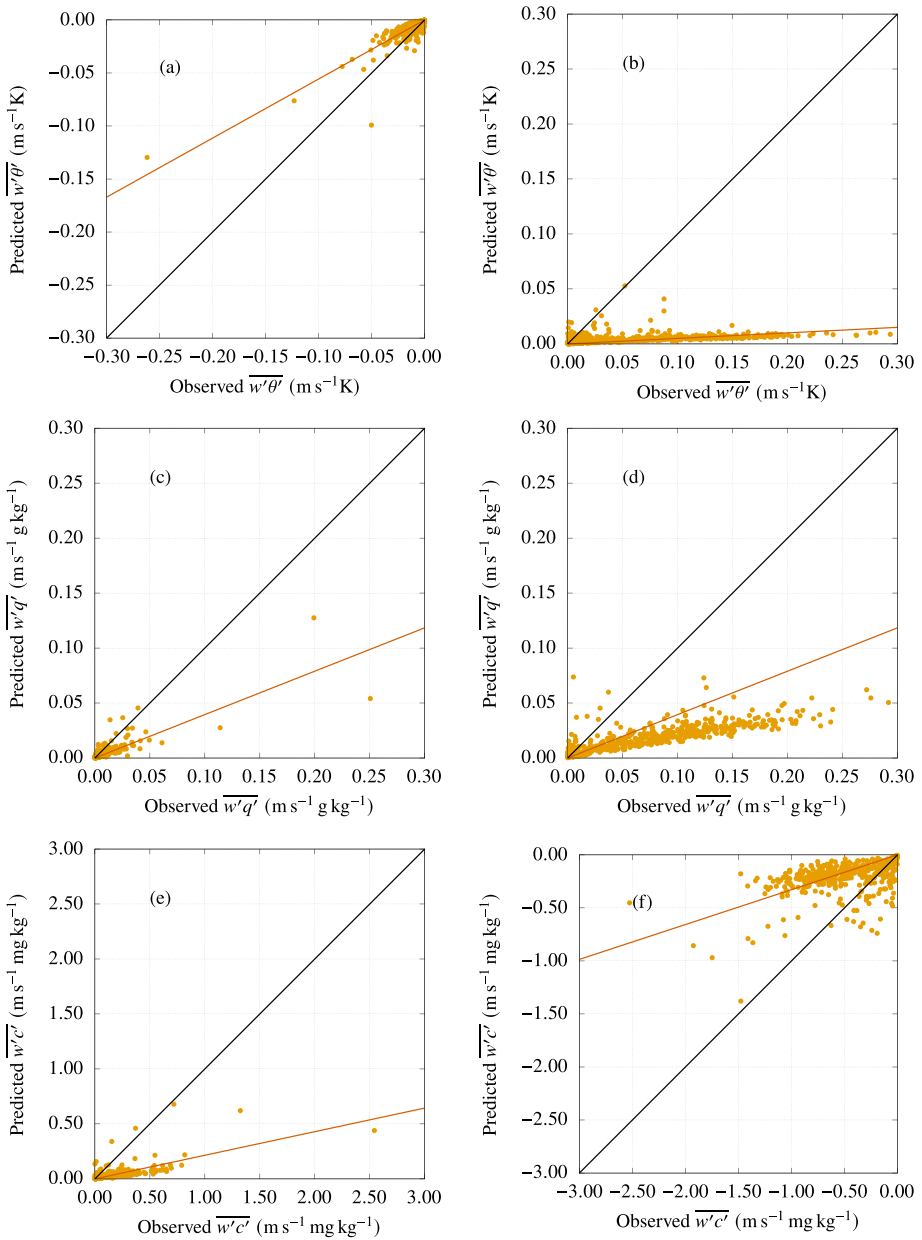
Fig. 5 Observed × predicted kinematic fluxes $\overline{w's'}$ by the variance method, $s = \theta$ (**a, b**), $s = q$ (**c, d**) and $s = c$ (**e, f**) for stable (**a, c, e**) and unstable (**b, d, f**) conditions. The vermillion line is a least-squares fit through the origin, and the black line is $y = x$

Table 5 Performance statistics for the kinematic fluxes $\overline{w'\theta'}$ (m s^{-1}K), $\overline{w'q'}$ (m s^{-1} g kg^{-1}), $\overline{w'c'}$ (m s^{-1} mg kg^{-1}), estimated by the variance method

Variable	r	C_d	BIAS	NBIAS	MAE	NMAE	RMSE	NRMSE	d_r
Stable conditions									
$\overline{w'\theta'}$	0.8623	0.6151	0.0037	0.3632	0.0051	0.5002	0.0093	0.9105	0.6623
$\overline{w'q'}$	0.8171	0.4895	-0.0040	-0.4897	0.0048	0.5802	0.0132	1.6091	0.6896
$\overline{w'c'}$	0.6657	-0.0687	-0.1221	-0.7706	0.1261	0.7960	0.2036	1.2850	0.4853
Unstable conditions									
$\overline{w'\theta'}$	0.3913	-0.7875	-0.0558	-0.9257	0.0564	0.9351	0.0816	1.3532	0.4526
$\overline{w'q'}$	0.7894	-0.7349	-0.0610	-0.7595	0.0624	0.7780	0.0798	0.9949	0.3779
$\overline{w'c'}$	0.5118	-0.3185	0.2778	0.5962	0.3207	0.6882	0.4229	0.9074	0.4689

BIAS, MAE and RMSE are given in the same corresponding units

fluxes tend to have a small spread around the median, but that the spread of the small magnitude fluxes is exceptionally large: we are truncating the vertical axes at a maximum value of 10, but larger ratios do occur in the dataset. Clearly, if we restrict the conditions so that only larger flux values are probed, the variance method will tend to perform better in the RSL: this is very likely what happened for small zenith angles in Zahn et al. (2016b). The physical mechanism explaining this is probably that, for large-magnitude fluxes, gradient production of scalar semivariance will be strong enough to balance, approximately, molecular dissipation of scalar variance.

5.2 Flux Estimates from REA-S

We applied REA-S for all 3 scalars using the median β_s for each scalar and for each stability range (stable, unstable) to estimate the fluxes. β_s estimation and flux performance used the same dataset, since as mentioned earlier the intent is only to assess the relative potential of the method. The median values of the obtained β_ss are listed in Table 6. The values of β_s are remarkably close under each stability regime. They are also clearly different in stable (mean of 0.6049) and unstable (mean of 0.5564) conditions. While analyzing the REA method at the same site with a different dataset, Zahn et al. (2016b) obtained similar values for β_s under unstable conditions, namely a mean of 0.5287 between the medians of β_θ, β_q and β_c at 39.4 m and 0.5847 at 81.6 m. Thus, it appears that β_s increases slightly with height in the RSL over the canopy in unstable conditions.

Figure 7 shows the predicted *versus* observed fluxes thus obtained: for each scalar, we predicted the flux with the corresponding median β_s in Table 6. The performance is very

Table 6 Median β_s, for $s = \theta, q, c$, under stable and unstable conditions

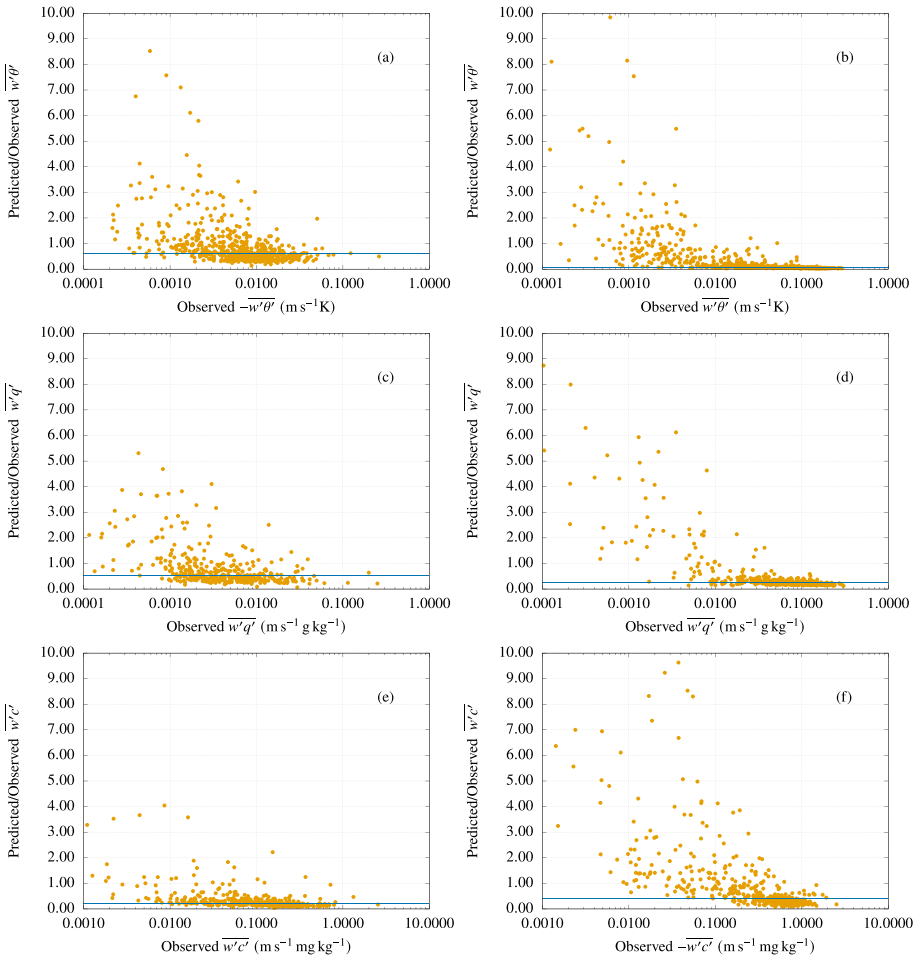| Scalar	Stable	Unstable
θ	0.6090	0.5478
q	0.6046	0.5631
c	0.6021	0.5582
Mean	0.6052	0.5564

Fig. 6 Observed ratios of predicted to observed kinematic fluxes $\overline{w's'}$ by the variance method, $s = \theta$ (**a, b**), $s = q$ (**c, d**) and $s = c$ (**e, f**) versus the observed fluxes, for stable (**a, c, e**) and unstable (**b, d, f**) conditions. The blue line is the median

good, showing an excellent agreement. Note that the small variability of β_s among all scalars for the same stability conditions gives confidence on the applicability of the method, without calibration, at least for the ATTO site—but bear in mind the β_s dependency on height. The relative errors of REA-S can be better discerned in Fig. 8. The scatter of the small magnitude fluxes is now much smaller than in Fig. 6 for the variance method, but it is still present, and also likely due, at least in part, to the inherently more difficult RSL conditions. The scatter is larger for stable than for unstable conditions. Together, Figs. 7 and 8 reconcile the previous results of Zahn et al. (2016b) and Zahn et al. (2023): plotted on an $x \times y$ graph, the REA method shows excellent performance, but this kind of plot hides the still large variability of the computed β_ss when plotted (for example) against ζ. Therefore, while the REA method is probably good enough for mean flux estimates over (say) many days, one must be cautious when the small-magnitude fluxes are of importance (say, for specific biophysical processes, etc.).
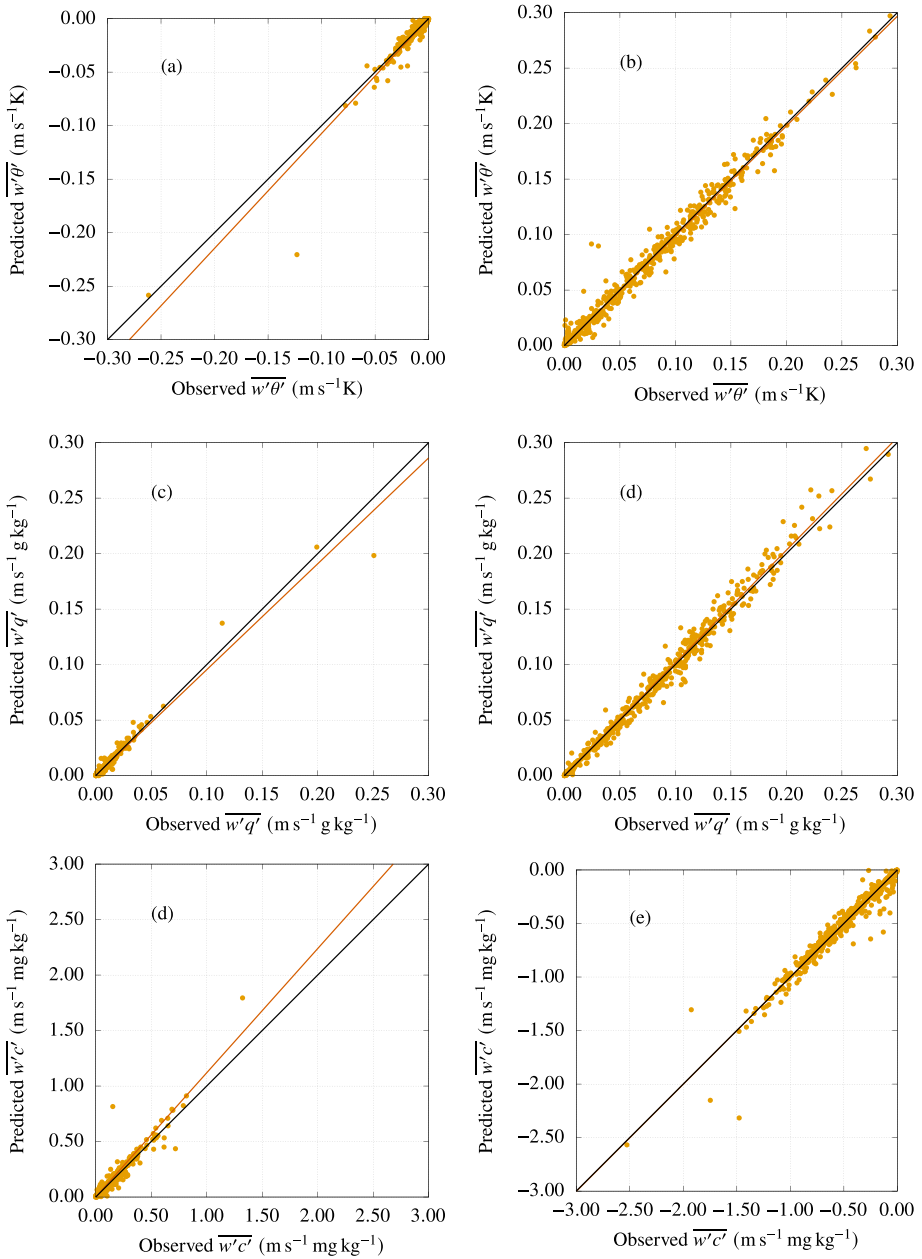
Fig. 7 Observed × predicted kinematic fluxes $\overline{w's'}$ by means of the REA-S method, $s = \theta$ (**a, b**), $s = q$ (**c, d**) and $s = c$ (**e, f**) for stable (**a, c, e**) and unstable (**b, d, f**) conditions. The vermillion line is a least-squares fit through the origin, and the black line is $y = x$

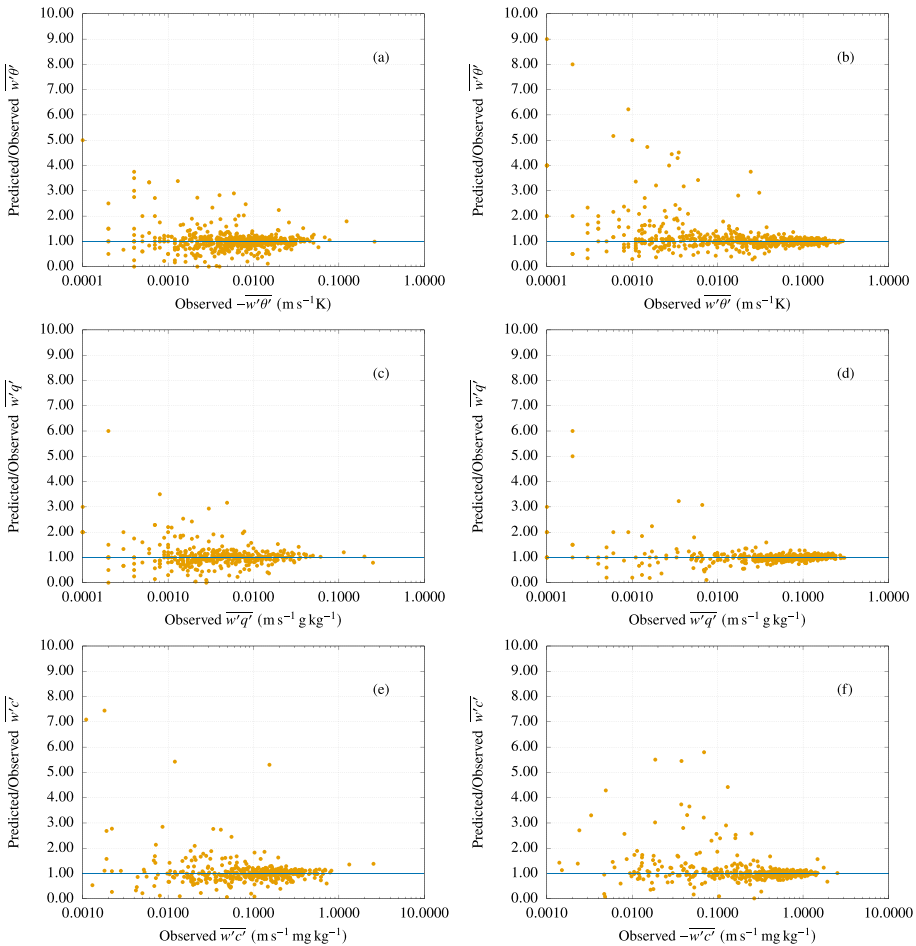**Fig. 8** Observed ratios of predicted to observed kinematic fluxes $\overline{w's'}$ by means of the REA-S method, $s = \theta$ (**a, b**), $s = q$ (**c, d**) and $s = c$ (**e, f**) versus the observed fluxes, for stable (**a, c, e**) and unstable (**b, d, f**) conditions. The blue line is the median

The errors of REA-S are quantified in Table 7. They are much smaller than those from the variance method (see Table 5), confirming in general the findings of Zahn et al. (2023), but now for an Amazonian RSL. Note that by estimating β_s as the median value, BIAS is virtually eliminated; NMAE remains below 10% for unstable conditions, and below $\sim 15\%$ for stable conditions.

5.3 Flux Estimates from REA-T

We applied REA-T for q and c with simultaneous measurement of β_θ, assuming $\beta_{q,c} = \beta_\theta$, and then estimating $\overline{w'q'}$ and $\overline{w'c'}$, for each stability regime (stable, unstable). This mimics the simultaneous measurement of sonic temperature, and dispenses with any *a priori* estimate of β_s, but has a built-in assumption of θ–s scalar similarity. Figure 9 shows the predicted versus observed fluxes thus obtained. The performance again is very good. The relative

Table 7 Performance statistics for the kinematic fluxes $\overline{w'\theta'}$ (m s^{-1}K), $\overline{w'q'}$ (m s^{-1} g kg^{-1}), $\overline{w'c'}$ (m s^{-1} mg kg^{-1}), estimated by REA-S

Variable	r	C_d	BIAS	NBIAS	MAE	NMAE	RMSE	NRMSE	d_r
Stable conditions									
$\overline{w'\theta'}$	0.9615	0.8921	−0.0002	−0.0214	0.0016	0.1604	0.0049	0.4821	0.8917
$\overline{w'q'}$	0.9820	0.9638	0.0001	0.0123	0.0013	0.1567	0.0035	0.4283	0.9162
$\overline{w'c'}$	0.9672	0.8735	0.0053	0.0337	0.0248	0.1563	0.0701	0.4421	0.8989
Unstable conditions									
$\overline{w'\theta'}$	0.9926	0.9853	−0.0002	−0.0035	0.0045	0.0742	0.0074	0.1228	0.9565
$\overline{w'q'}$	0.9931	0.9845	0.0007	0.0084	0.0051	0.0632	0.0075	0.0939	0.9495
$\overline{w'c'}$	0.9768	0.9528	−0.0039	−0.0085	0.0423	0.0908	0.0800	0.1716	0.9299

BIAS, MAE and RMSE are given in the same corresponding units
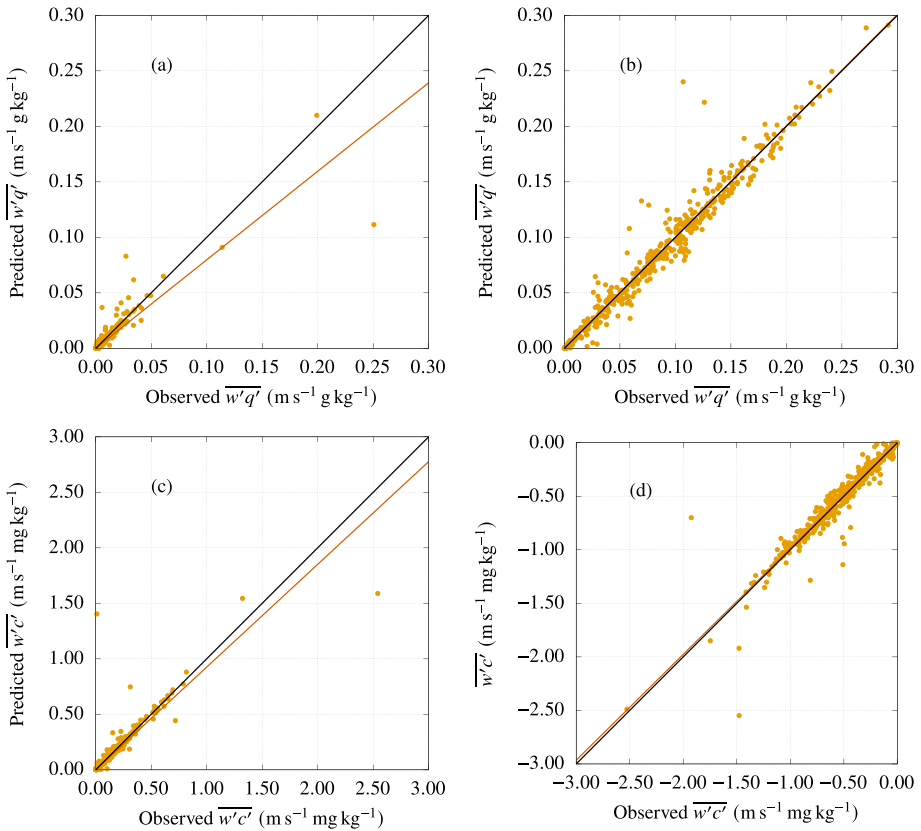
Fig. 9 Observed × predicted kinematic fluxes $\overline{w's'}$ by means of the REA-T method, $s = q$ (**a, b**) and $s = c$ (**c, d**) for stable (**a, c**) and unstable (**b, d**) conditions. The vermillion line is a least-squares fit through the origin, and the black line is $y = x$
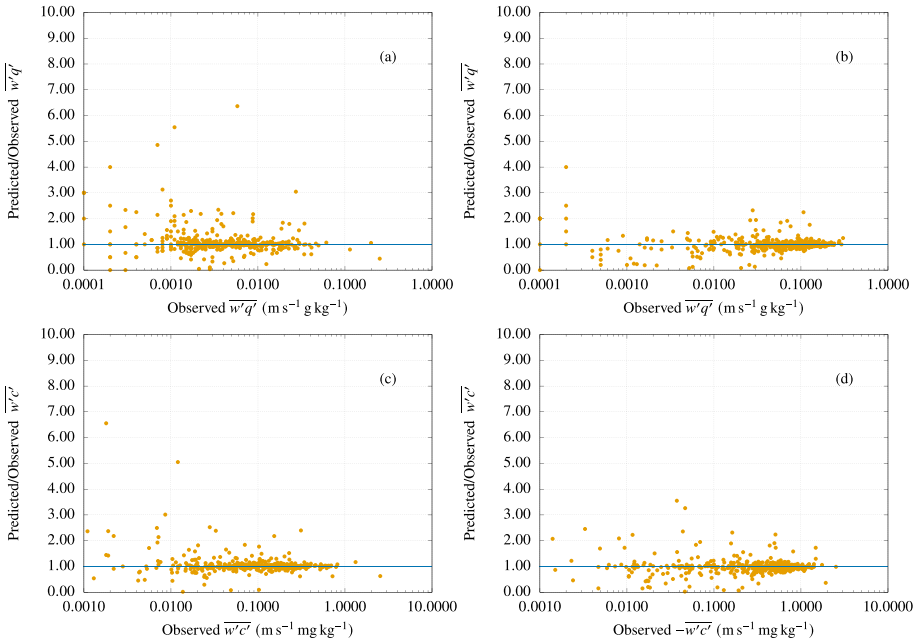
Fig. 10 Observed ratios of predicted to observed kinematic fluxes $\overline{w's'}$ by means of the REA-T method, $s = q$ (**a, b**) and $s = c$ (**c, d**) versus the observed fluxes, for stable (**a, c**) and unstable (**b, d**) conditions. The blue line is the median

Table 8 Performance statistics for the kinematic fluxes $\overline{w'q'}$ (m s^{-1} g kg^{-1}), $\overline{w'c'}$ (m s^{-1} mg kg^{-1}), estimated by REA-T

Variable	r	C_d	BIAS	NBIAS	MAE	NMAE	RMSE	NRMSE	d_r
Stable conditions									
$\overline{w'q'}$	0.8948	0.7982	0.0000	0.0045	0.0018	0.2209	0.0084	1.0122	0.8823
$\overline{w'c'}$	0.8949	0.7961	0.0044	0.0276	0.0186	0.1171	0.0893	0.5612	0.9243
Unstable conditions									
$\overline{w'q'}$	0.9789	0.9547	0.0002	0.0022	0.0069	0.0840	0.0128	0.1555	0.9304
$\overline{w'c'}$	0.9617	0.9208	0.0047	0.0098	0.0458	0.0962	0.1036	0.2176	0.9239

BIAS, MAE and RMSE are given in the same corresponding units

errors of REA-T can be discerned in Fig. 10. Figures 9 and 10 look very similar to Figs. 7 and 8, showing that both REA-S and REA-T produce reasonably good results. The same observations about the large scatter of the predicted fluxes when their magnitude is small apply. The performance statistics in Table 8 are somewhat worse than their counterparts in Table 7, but by a small margin only. Therefore, we deem REA-T as capable as REA-S with the additional advantage that no *a priori* estimate of β_s is necessary.

5.4 Long-Term Hourly Predictive Ability of REA

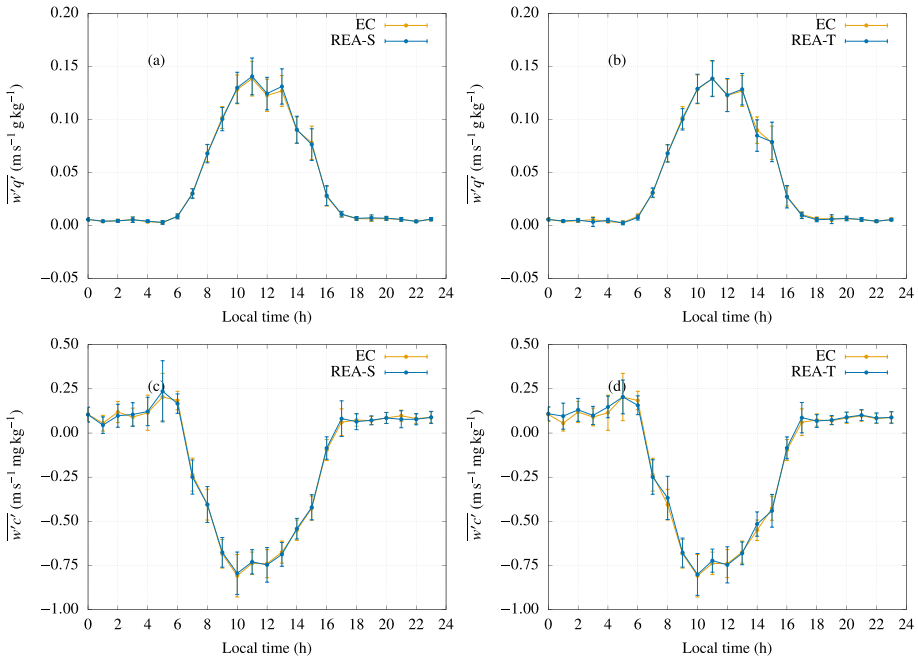Figure 11 shows the hourly means for the whole dataset, for both $s = q$ and $s = c$, for

Fig. 11 Hourly means of EC, REA-S and REA-T fluxes at the ATTO site. The bars indicate 1 standard deviation around the means: **a** EC × REA-S, $s = q$; **b** EC × REA-T, $s = q$; **c** EC × REA-S, $s = c$; **d** EC × REA-T, $s = c$

REA-S (a, c) and REA-T (b, d) against eddy covariance measurements. The performance of REA-S for $s = \theta$ is very similar to that exhibited for q and c and is not shown while REA-T for temperature, obviously, makes no sense. As it can be seen, the REA method's (both versions) ability to capture the daily cycle and its dispersion around the hourly means is very similar to the eddy covariance measurements themselves. For the purpose of quantifying mass exchanges between the canopy and the atmosphere at the ATTO site (and very likely many other similar forested regions), therefore, our results validate the use of REA as a valuable alternative when fast-response scalar sensors are not available. The one caveat is whether these results also apply for *trace* gases such as CH_4 or isoprene since, if their fluxes are all very small, they might fall in the high scatter region of Figs. 8 and 10. In all fairness, the good performance of the REA method over forests is not reported here for the first time; it can be found in Bowling et al. (1999) for water vapor and CO_2 fluxes (*c.f.* their Fig. 5a–d). At the same they also show that the scatter of the REA method in comparison to eddy covariance is considerably larger for isoprene flux (*c.f.* their Fig. 5e, f)—although this may also be a consequence of the precision of their isoprene measurements. Clearly, the subject of the ability of the REA method to produce consistently good results for trace gases will require further study.

6 Discussion and Conclusions

The relatively large scatter found for β_s by Zahn et al. (2016b) at the same site (ATTO) as the present study's might suggest that the REA method is not applicable in the RSL of ATTO.

However, the recent finding of Zahn et al. (2023) that the REA can yield rather good results in comparison to EC measurements even when the scalar in question (in their case, mostly CO_2) does not conform to MOST, has prompted us to re-visit the issue with ATTO data. The present work actually reconciles both findings. The β_s scatter *is* large in the RSL, as can be seen (indirectly) in Figs. 8 and 10. On the other hand, this affects mostly the small-magnitude fluxes. Zahn et al. (2023) showed very clearly that when any scalar "fails" MOST this is basically caused by relatively large (in their case) transport and storage terms: at the ATTO site, other causes such as horizontal and vertical advection might also be playing a role, on account of the underlying topography (see Chamecki et al. 2020; Allouche et al. 2022). In all likelihood, the failure is associated with the small-magnitude fluxes because then the corresponding gradient production term in the scalar semivariance budget is also *relatively* small and the other terms are causing the breakdown of MOST. The term "relatively" is key here, since (again, very likely) the gradient production ultimately is small with respect to the scalar dissipation term. This, however, remains a conjecture and will need to be addressed in future research studies.

Large-magnitude fluxes that occur in the middle of the day, on the other hand, are (again in all likelihood, pending a detailed analysis of the scalar semivariance budgets) associated with a large gradient production term. In this case the β_ss approach the approximately constant values around 0.6 found elsewhere in the literature when measurements were made in the ISL. This is exactly what Zahn et al. (2016b) found for small zenith angles, which naturally occur in the middle of the day, although an explanation based on the scalar semivariance budget was not offered then. These large-magnitude fluxes weigh more heavily in most performance statistics or visual analyses, which tend to hide the large scatter of the small-magnitude fluxes. Moreover, when hourly averages of all data were taken, in Fig. 11, the REA method showed considerable ability in reproducing the daily cycle of the EC measurements for the dry season. This lends confidence in the ability of the REA method, despite the shortcomings of RSL-measurements related to the small-magnitude fluxes, of producing reliable estimates of the canopy-atmosphere mass exchanges over timescales larger than (say) several days. In particular, REA-T seems to be a better choice than REA-S since, in spite of slightly larger overall errors, it dispenses with *a priori* assumptions on the value of β_s.

However, to really settle the matter, further research needs to be done:

1. A better understanding of the interplay between the scalar semivariance budget and REA needs to be obtained. For this purpose, a budget as detailed as possible is needed in conjunction with the behavior of β_s under various situations, *viz.* when the gradient production term is large, and when the transport term is large or more generally when a large imbalance between gradient production and dissipation is present.
2. Unfortunately, a criterion for identifying such imbalance that dispenses with EC measurements is lacking; such a criterion would be highly useful for practical quality control of REA measurements. The scalar flux number proposed by Cancelli et al. (2012) might be a useful starting point for this purpose.
3. Scalar variance budgets involving trace gases measured by EC and simultaneous assessment of the REA for these gases are also needed. The present study considered scalars associated with intuitively large fluxes of heat, H_2O and CO_2. A possibility remains that for trace gases the gradient production term is never able to balance dissipation alone. If this happens, then, the REA method is bound to become much more uncertain.

Author Contributions NLD conceived the overall research. NLD, IMCT, CQD, LM and DB all processed data and generated figures. NLD wrote the manuscript. All authors reviewed the manuscript.

Declarations

Conflict of interest The authors declare no competing interests.

References

Allouche M, Bou-Zeid E, Ansorge C, Katul GG, Chamecki M, Acevedo O, Thanekar S, Fuentes JD (2022) The detection, genesis, and modeling of turbulence intermittency in the stable atmospheric surface layer. J Atmos Sci 79:1171–1190

Andreae MO, Acevedo OC, Araújo A, Artaxo P, Barbosa CGG, Barbosa HMJ, Brito J, Carbone S, Chi X, Cintra BBL, da Silva NF, Dias NL, Dias-Júnior CQ, Ditas F, Ditz R, Godoi AFL, Godoi RHM, Heimann M, Hoffmann T, Kesselmeier J, Könemann T, Krüger ML, Lavric JV, Manzi AO, Lopes AP, Martins DL, Mikhailov EF, Moran-Zuloaga D, Nelson BW, Nölscher AC, Santos Nogueira D, Piedade MTF, Pöhlker C, Pöschl U, Quesada CA, Rizzo LV, Ro CU, Ruckteschler N, Sá LDA, de Oliveira Sá M, Sales CB, dos Santos RMN, Saturno J, Schöngart J, Sörgel M, de Souza CM, de Souza RAF, Su H, Targhetta N, Tóta J, Trebs I, Trumbore S, van Eijck A, Walter D, Wang Z, Weber B, Williams J, Winderlich J, Wittmann F, Wolff S, Yáñez-Serrano AM (2015) The Amazon Tall Tower Observatory (ATTO): overview of pilot measurements on ecosystem ecology, meteorology, trace gases, and aerosols. Atmos Chem Phys 15:10723–10776. https://doi.org/10.5194/acp-15-10723-2015

Baker J, Norman J, Bland W (1992) Field-scale application of flux measurement by conditional sampling. Agric For Meteorol 62:31–52. https://doi.org/10.1016/0168-1923(92)90004-N

Bowling DR, Turnipseed AA, Delany A, Baldocchi DD, Greenberg JP, Monson R (1998) The use of relaxed eddy accumulation to measure biosphere-atmosphere exchange of isoprene and other biological trace gases. Oecologia 116:306–315. https://doi.org/10.1007/s004420050592

Bowling D, Delany A, Turnipseed A, Baldocchi D, Monson R (1999) Modification of the relaxed eddy accumulation technique to maximize measured scalar mixing ratio differences in updrafts and downdrafts. J Geophys Res Atmos 104:9121–9133. https://doi.org/10.1029/1999JD900013

Businger JA, Oncley SP (1990) Flux measurement with conditional sampling. J Atmos Ocean Technol 7:349–352. https://doi.org/10.1175/1520-0426(1990)007<0349:FMWCS>.0.CO;2

Cancelli DM, Dias NL, Chamecki M (2012) Dimensionless criteria for the production-dissipation equilibrium of scalar fluctuations and their implications for scalar similarity. Water Resour Res 48:W10522. https://doi.org/10.1029/2012WR012127

Chamecki M, Freire LS, Dias NL, Chen B, Dias-Junior CQ, Toledo Machado LA, Sörgel M, Tsokankunku A, Araújo A (2020) Effects of vegetation and topography on the boundary layer structure above the amazon forest. J Atmos Sci 77:2941–2957. https://doi.org/10.1175/JAS-D-20-0063.1

Chor TL, Dias NL, Araújo A, Wolff S, Zahn E, Manzi A, Trebs I, Sá MO, Teixeira PR, Sörgel M (2017) Flux-variance and flux-gradient relationships in the roughness sublayer over the Amazon forest. Agric For Meteorol 239:213–222. https://doi.org/10.1016/j.agrformet.2017.03.009

Desjardins RL (1972) A study of carbon-dioxide and sensible heat fluxes using the eddy correlation technique. Ph.D. thesis, Cornell University

Desjardins RL (1977) Description and evaluation of a sensible heat flux detector. Boundary-Layer Meteorol 11:147–154. https://doi.org/10.1007/BF02166801

Dias NL (2013) Research on atmospheric turbulence by Wilfried Brutsaert and collaborators. Water Resour Res 49:7169–7184. https://doi.org/10.1002/wrcr.20461

Dias NL, Brutsaert W (1996) Similarity of scalars under stable conditions. Boundary-Layer Meteorol 80:355–373. https://doi.org/10.1007/BF00119423

Dias NL, Hong J, Leclerc M, Black Nesic Z, Krishnan P (2009) A simple method of estimating scalar fluxes over forests. Boundary-Layer Meteorol 132:401–414. https://doi.org/10.1007/s10546-009-9408-0

Dias-Júnior CQ, Dias NL, dos Santos RMN, Sörgel M, Araújo A, Tsokankunku A, Ditas F, de Santana RA, von Randow C, Sá M et al (2019) Is there a classical inertial sublayer over the amazon forest? Geophys Res Lett 46:5614–5622. https://doi.org/10.1029/2019GL083237

Edson JB, Fairall CW, Bariteau L, Zappa CJ, Cifuentes-Lorenzen A, McGillis WR, Pezoa S, Hare JE, Helmig D (2011) Direct covariance measurement of CO2 gas transfer velocity during the 2008 southern ocean gas exchange experiment: wind speed dependency. J Geophys Res Oceans 116:C00F10. https://doi.org/10.1029/2011JC007022

Fuentes JD, Chamecki M, dos Santos RMN, von Randow C, Stoy PC, Katul G, Fitzjarrald D, Manzi A, Gerken T, Trowbridge A, Freire LS, Ruiz-Plancarte J, Maia JMF, Tóta J, Dias NL, Fisch G, Schumacher C, Acevedo O, Mercer JR (2016) Linking meteorology, turbulence, and air chemistry in the amazon rainforest. Bull Am Meteorol Soc 97:2329–2342. https://doi.org/10.1175/BAMS-D-15-00152.1

Hill RJ (1989) Implications of Monin–Obukhov similarity theory for scalar quantities. J Atmos Sci 46:2236–2244. https://doi.org/10.1175/1520-0469(1989)046<2236:IOMSTF>2.0.CO;2

Katul G, Peltola O, Grönholm T, Launiainen S, Mammarella I, Vesala T (2018) Ejective and sweeping motions above a peatland and their role in relaxed-eddy-accumulation measurements and turbulent transport modelling. Boundary-Layer Meteorol 169:163–184. https://doi.org/10.1007/s10546-018-0372-4

McMillen RT (1988) An eddy correlation technique with extended applicability to non-simple terrain. Boundary-Layer Meteorol 43:231–245. https://doi.org/10.1007/BF00128405

Mochizuki T, Tani A, Takahashi Y, Saigusa N, Ueyama M (2014) Long-term measurement of terpenoid flux above a Larix kaempferi forest using a relaxed eddy accumulation method. Atmos Environ 83:53–61. https://doi.org/10.1016/j.atmosenv.2013.10.054

Mortarini L, Katul GG, Cava D, Dias-Junior CQ, Dias NL, Manzi A, Sorgel M, Araújo A, Chamecki M (2023) Adjustments to the law of the wall above an amazon forest explained by a spectral link. Phys Fluids. https://doi.org/10.1063/5.0135697

Ren X, Sanders J, Rajendran A, Weber R, Goldstein A, Pusede S, Browne E, Min KE, Cohen R (2011) A relaxed eddy accumulation system for measuring vertical fluxes of nitrous acid. Atmos Meas Tech 4:2093–2103. https://doi.org/10.5194/amt-4-2093-2011

Rhew RC, Deventer MJ, Turnipseed AA, Warneke C, Ortega J, Shen S, Martinez L, Koss A, Lerner BM, Gilman JB et al (2017) Ethene, propene, butene and isoprene emissions from a ponderosa pine forest measured by relaxed eddy accumulation. Atmos Chem Phys 17:13417–13438. https://doi.org/10.5194/acp-17-13417-2017

Santana RA, Dias-Júnior CQ, da Silva JT, Fuentes JD, do Vale RS, Alves EG, dos Santos RMN, Manzi AO (2018) Air turbulence characteristics at multiple sites in and above the amazon rainforest canopy. Agric For Meteorol 260:41–54. https://doi.org/10.1016/j.agrformet.2018.05.027

Sarkar C, Turnipseed A, Shertz S, Karl T, Potosnak M, Bai J, Serça D, Bonal D, Burban B, Lopes PR et al (2020) A portable, low-cost relaxed eddy accumulation (REA) system for quantifying ecosystem-level fluxes of volatile organics. Atmos Environ 242:117764. https://doi.org/10.1016/j.atmosenv.2020.117764

Webb EK, Pearman GI, Leuning R (1980) Correction of flux measurements for density effects due to heat and water vapor transfer. Q J R Meteorol Soc 106:85–100. https://doi.org/10.1002/qj.49710644707

Willmott CJ, Robeson SM, Matsuura K (2012) A refined index of model performance. Int J Climatol 32:2088–2094. https://doi.org/10.1002/joc.2419

Zahn E, Chor TL, Dias NL (2016) A simple methodology for quality control of micrometeorological datasets. Am J Environ Eng 6:135–142. https://doi.org/10.5923/s.ajee.201601.20

Zahn E, Dias NL, Araújo A, Sá LDA, Sörgel M, Trebs I, Wolff S, Manzi A (2016) Scalar turbulent behavior in the roughness sublayer of an Amazonian forest. Atmos Chem Phys 16:11349–11366. https://doi.org/10.5194/acp-16-11349-2016

Zahn E, Bou-Zeid E, Dias NL (2023) Relaxed eddy accumulation outperforms Monin–Obukhov flux models under non-ideal conditions. Geophys Res. https://doi.org/10.1029/2023GL103099

Zhu T, Pattey E, Desjardins R (2000) Relaxed eddy-accumulation technique for measuring ammonia volatilization. Environ Sci Technol 34:199–203. https://doi.org/10.1021/es980928f